Square Packing and Structural Arrangement of ABC Triblock Copolymer Spheres in Thin Films

Chuanbing Tang,[†] Joona Bang,[‡] Gila E. Stein,[||] Glenn H. Fredrickson,[†,||] Craig J. Hawker,*[,†,§,⊥] Edward J. Kramer,*[,†,§,||] Michael Sprung,[#] and Jin Wang[#]

Materials Research Laboratory, University of California, Santa Barbara, California 93106; Department of Chemical and Biological Engineering, Korea University, Seoul 136-701, Republic of Korea; Department of Materials, University of California, Santa Barbara, California 93106; Department of Chemical Engineering, University of California, Santa Barbara, California 93106; Department of Chemistry and Biochemistry, University of California, Santa Barbara, California 93106; and Advanced Photon Source, Argonne National Laboratory, Argonne, Illinois 60439

Received January 28, 2008; Revised Manuscript Received March 17, 2008

ABSTRACT: Nanoporous thin films were prepared from poly(ethylene oxide)-*b*-poly(methyl methacrylate)-*b*-polystyrene (PEO-*b*-PMMA-*b*-PS) ABC triblock copolymer by solvent annealing under high relative humidity followed by UV degradation and acid washing. Ordered half-spheres at the surface that template ordering of spheres below the surface in thin films were formed as a result of the interaction between the hydrophilic PEO segments and water vapor during processing. The spherical block copolymer domains exhibit complex packing behavior on the surface and in the interior. A half-sphere "monolayer" and a half-sphere plus whole sphere "bilayer" were formed in thin films with thicknesses of 43 and 71 nm, respectively, and have hexagonal lattice symmetry. For half-sphere plus two whole sphere "trilayers" with a nominal thickness of 117 nm, coexistence of regions of hexagonal and square packing was observed by transmission electron microscopy, scanning force microscopy, scanning electron microscopy, and grazing-incidence small-angle X-ray scattering. Square packing was consistent with a surface-truncated unit cell of a body-centered cubic lattice with the (100) plane parallel to the surface.

Introduction

The self-assembly of block copolymers in thin films has drawn much attention due to its potential applications in microelectronic devices, data storage system, membranes, etc.[1–5] Ordered arrays of spheres, cylinders, and lamellae with controlled size and center-to-center distance can be achieved through manipulation of molecular weight, block volume fractions, and segment−segment interactions, i.e., the Flory parameter χ.[6,7] In thin films, 2D confinement and surface/substrate interactions are additional key parameters that affect ordering behavior.[8,9] In order to induce both orientational and positional ordering of thin film block copolymer domains, many strategies have been developed that use for example electric fields,[10] graphoepitaxy,[11,12] shear,[13,14] neutral surfaces,[15,16] chemically patterned substrates,[17] solution evaporation,[18] zone casting,[19] and crystallization.[20]

While the ordering of cylindrical and lamellar block copolymer films have been extensively explored, block copolymers with spherical domains also present an interesting model system for investigating ordering behavior in thin films.[21–24] It is well-established from transmission electron microscopy (TEM) and small-angle X-ray scattering (SAXS) studies that block copolymer spheres adopt an equilibrium body-centered cubic (BCC) arrangement in the bulk.[25–27] However, when confined to a 2D thin film monolayer, the equilibrium structure of spheres is close-packed hexagonal (HEX). The different ordered arrangement of diblock copolymer spheres in two dimensions and in three dimensions can be explained by a competition between the tendency to minimize any nonuniform deformation of the matrix chains that need to fill the matrix space and the tendency to maintain uniform interfacial curvature to minimize block−block interfacial energy.[27–29]

Recently, Stein et al. reported in detail on the transition from 2D to 3D packing in spherical-domain block copolymers under equilibrium thermal annealing using a combination of grazing-incidence small-angle X-ray scattering (GISAXS) and TEM techniques.[30] They found hexagonal symmetry in films 1, 2, 3, and 4 layers thick with the close-packed planes of spheres exhibiting A, AB, ABA, and ABAB stacking. At 5 layers, the hexagonal symmetry breaks to form an orthorhombic phase, characterized by the ratio of second/first nearest-neighbors distances a_1/a_2 and the lattice angle φ. As the number of layers is increased, a_1/a_2 and φ increase continuously to approach their corresponding values for BCC (110) planes. Self-consistent-field theory calculations provide a semiquantitative description of the transition and the insight that it is a consequence of competition between the optimal HEX packing at the film surfaces with the preferred BCC (110) inner layer packing in the bulk.[31]

Among the strategies to induce ordering, directional solvent evaporation is very promising for submicron lithography due to its simplicity and low processing costs.[18,32–36] In principle, the rate of evaporation and evaporation-induced solvent flow can be manipulated to guide the orientated growth and positioning of microdomains. Evaporation results in a solvent concentration gradient, which induces the ordering that starts from the surface and propagates toward the interior and eventually throughout the entire film. Recently, the Russell group reported manipulation of the growth and orientation of polystyrene-*b*-poly(ethylene oxide) (PS-*b*-PEO) diblock copolymer cylinders perpendicular to the surface and substrate through solvent annealing under controlled humidity conditions.[37–39] The absence of good orientational ordering under low-humidity condi-

* Authors for correspondence. E-mail: edkramer@mrl.ucsb.edu or hawker@mrl.ucsb.edu.
[†] Materials Research Laboratory, University of California, SB.
[‡] Korea University.
[§] Department of Materials, University of California, SB.
[||] Department of Chemical Engineering, University of California, SB.
[⊥] Department of Chemistry and Biochemistry, University of California, SB.
[#] Argonne National Laboratory.

10.1021/ma800207n CCC: $40.75
Published on Web 05/28/2008

Scheme 1. Illustration of PEO-*b*-PMMA-*b*-PS Thin Film Solvent Annealing with Controlled Humidity

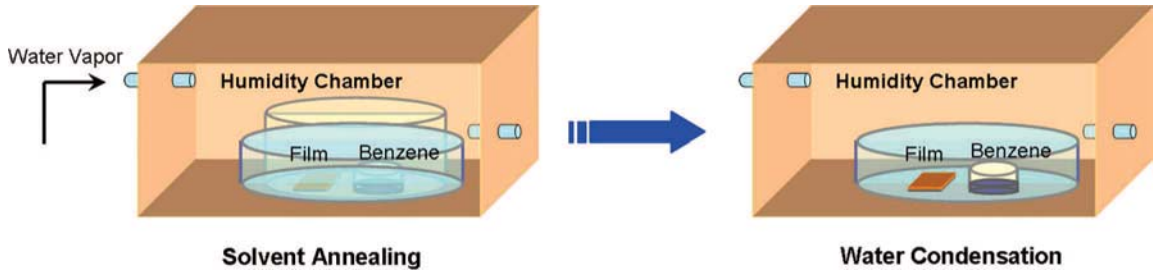

tions indicates that for block copolymers with a hydrophilic segment (PEO) the ordering mechanism is more complicated than that assumed by the description of directional solvent evaporation presented above. This view is further buttressed by PS and PEO block copolymers containing poly(methyl methacrylate) (PMMA) through either blending[38] or covalent bonding (e.g., ABC triblock copolymers[40]). In this case, the PEO blocks are believed to induce ordering whereas the PMMA functions as a sacrificial block to produce nanoporous materials under UV degradation. The importance of the PEO and its interaction with water is underlined by a recent report of a PEO/humidity controlled transition from a lamellar PEO-*b*-PMMA-*b*-PS triblock copolymer thin film at low humidity to a hexagonally perforated lamellar (HPL) structure with PEO perforations to the surface at high humidity.[41] A similar conclusion can be drawn from a report of the induction of the formation of oriented PMMA cylinders of a PS-*b*-PMMA block copolymer perpendicular to the film plane by adding PEO-coated Au nanoparticles to a solution that was processed by directional solvent evaporation under high-humidity conditions.[42] At low humidity, or at any humidity in the absence of the PEO-coated Au nanoparticles, no orientation and poor order were observed.

Multiple phenomena should be taken into account to explain the morphologies that result from solvent annealing. Solvent evaporation generates a concentration gradient normal to the surface. Microphase separation first takes place on the surface, generating an ordering front, which propagates through the whole film. The directionality of solvent evaporation can be used to explain the high orientational order of cylinders and lamellae normal to films provided that both domains order simultaneously at the surface. Such orientation has been reported by numerous groups[18,32,34,35,37,40] but requires that the surface energies of the domains be similar under the ordering conditions.

Traditionally, films of ordered spherical domains have been created by a slow thermal annealing process, which allows sufficient time for chain diffusion and structural reconstruction, and thus these films approach their thermodynamic equilibrium structure.[30,31,43–49] However, for the much faster process of solvent annealing and evaporation under controlled humidity, chains must diffuse and reorganize within a time several orders of magnitude shorter than those used for thermal processing. Under such conditions, the surface and interior reconstruction is unlikely to result in an equilibrium structure. The transformation of an equilibrium lamellar structure in PEO-*b*-PMMA-*b*-PS triblock copolymers to a nonequilibrium HPL structure under high-humidity solvent annealing is a case in point.[41]

It is well-known that ABC triblock copolymers have much richer and more complicated structures as compared to simple AB diblock copolymers.[6,50,51] While there have been many studies reported on theoretical modeling[52–55] or experimental design on ABC triblock copolymers,[56–58] there have been no experimental reports on the structural changes of ABC triblock spheres in the thin films.

Herein we utilize a solvent-annealing process under controlled humidity to induce ordering of films consisting of spherical domains of an ABC triblock copolymer. The surface layer of each film is actually a half-layer consisting of half-spheres at the surface with the bottom layer being a flat brush. We convert these films into nanoporous thin films by removing the blocks making up the spheres by UV degradation and determine the structural arrangement of these spherical domains in the films by using the complementary techniques scanning force microscopy (SFM), scanning electron microscopy (SEM), transmission electron microscopy (TEM), and grazing incidence small-angle X-ray scattering (GISAXS). The lattice packing of spherical domains in films consisting of $2^1/_2$ layers of spheres is body-centered cubic (BCC); however, in thinner films consisting of either a half-layer or $1^1/_2$ layers of spheres, the structure is close-packed hexagonal (HEX). For the $2^1/_2$ layers of spheres with a BCC structure, we observe a square packing consistent with the film surface being a (100) plane.

Experimental Section

Synthesis of Poly(ethylene oxide)-*b*-poly(methyl methacrylate)-*b*-styrene (PEO-*b*-PMMA-*b*-PS) Triblock Copolymers. The PEO-*b*-PMMA-*b*-PS ($EO_{114}MMA_{65}S_{433}$, $M_w/M_n = 1.07$) ABC triblock copolymers were synthesized using published methods.[40] In short, the material was synthesized by reversible addition fragmentation chain transfer polymerization (RAFT), in which a PEO RAFT macroinitiator was chain extended with PMMA, yielding a PEO−PMMA diblock copolymer macro chain transfer agent. Further chain extension with PS resulted in the desired ABC triblock copolymers. The number-average molecular weight M_n of each segment was determined by proton NMR based on the known M_n of the PEO macroinitiator and the characteristic signals corresponding to EO, MMA, and S units. The polydispersity index was obtained from gel permeation chromatography, which was performed in THF using a Waters chromatography system, equipped with four 5 μm Waters columns (300 × 7.7 mm) connected in series with increasing pore size (100, 1000, 10 000, and 1 000 000 Å), a Waters 410 differential refractometer index (DRI), and 996 photodiode array detectors, calibrated with linear PMMA and PS standards.

Preparation of Thin Films. The PEO-*b*-PMMA-*b*-PS triblock copolymers were spin-coated from benzene solutions onto silicon substrates coated with a 100 nm thick silicon oxide layer. The film thickness was controlled by simple adjustment of the solution concentration. The thin films were then solvent annealed under controlled humidity as illustrated in Scheme 1. The films were annealed overnight under saturated benzene vapor supplied by a neighboring solvent reservoir in a sealed chamber, an upside-down glass container on a larger Petrie dish, all of which was placed in a larger glovebox. The initial relative humidity in the sealed chamber was ~40%, the ambient humidity initially outside the glovebox. The inside of the glovebox was maintained at a constant relative humidity (RH) by flowing moist air from a humidifying system through it before placing the sealed chamber in it. Once the solvent annealing time had elapsed, the upside-down glass container was removed from the Petrie dish inside the much larger glovebox, thus allowing the benzene in the swollen film to evaporate under a given RH condition. Our earlier experiments demonstrated

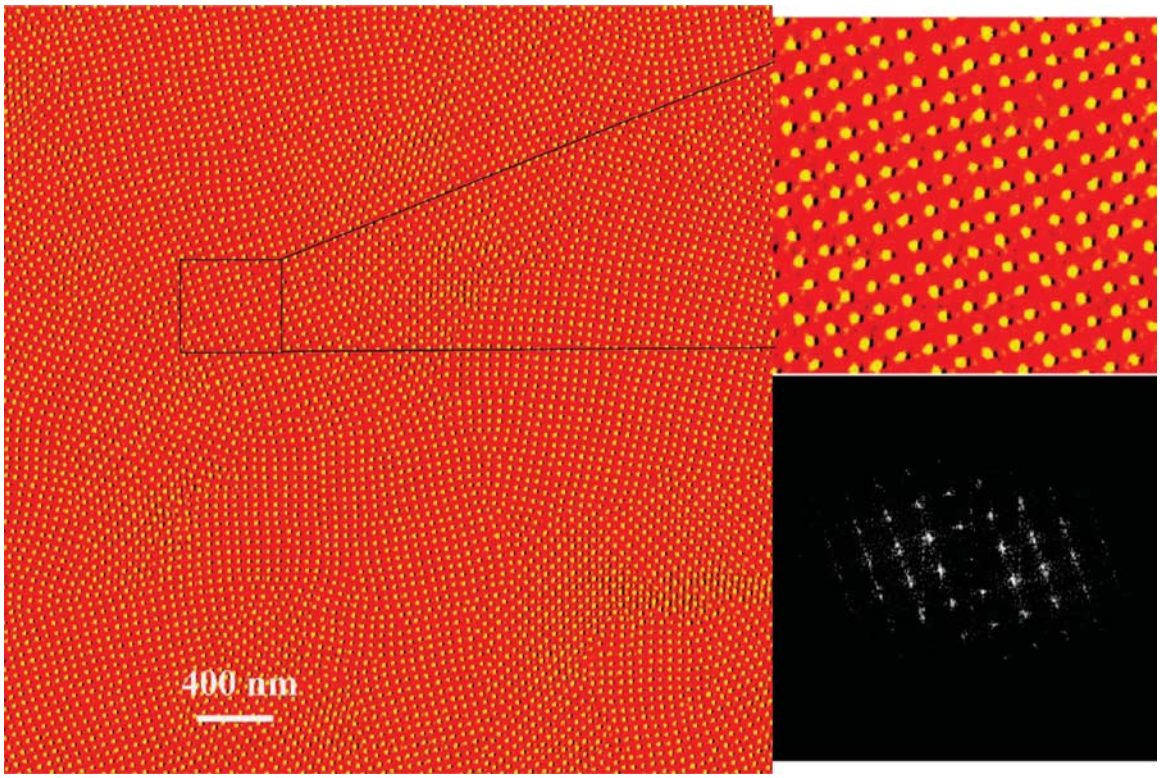

Figure 1. SFM phase images of square surface domain packing from 117 nm thick PEO-*b*-PMMA-*b*-PS films after annealing for 16 h under saturated benzene vapor at a relative humidity of ~80−90%. Inset: magnified square array and corresponding Fourier transform.

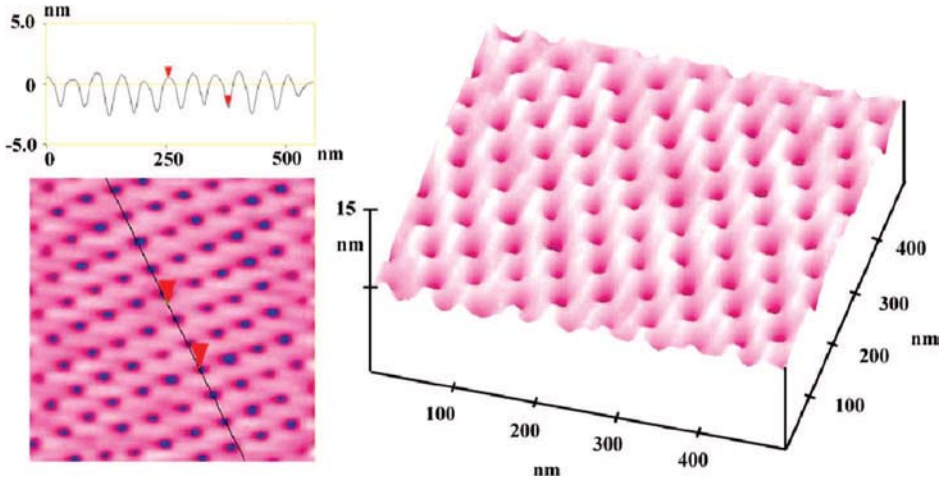

Figure 2. SFM topographical height image and section analysis of square packing from PEO-*b*-PMMA-*b*-PS thin films with thickness 117 nm after annealing for 16 h under saturated benzene vapor and high humidity.

that keeping the relative humidity at ~90% induces good lateral ordering of surface PEO domains.[40] After the solvent annealing process, selected films were exposed to deep UV light (254 nm) at a dose of 25 J cm^{-2} (XX-15S, UVP Inc.) under vacuum for 10 min followed by washing with acetic acid and water. The structure of other films was probed without UV degradation and washing.

Scanning Force Microscopy (SFM). Tapping mode SFM experiments were carried out using either a Multimode Nanoscope III system (Digital Instruments, Santa Barbara, CA) or a MFP-3D stand-alone system (Asylum Research, Santa Barbara, CA). The measurements were performed using commercial Si cantilevers with a nominal spring constant and resonance frequency equal to 48 N/m and 190 kHz, respectively, or 3 N/m and 60 kHz, respectively (ACL or FORTA, Applied Nanostructures, Santa Clara, CA). The height and phase images were acquired simultaneously at the set-point ratio $A/A_0 = 0.9-0.95$, where A and A_0 refer to the "tapping" and "free" cantilever amplitudes, respectively.

Scanning Electron Microscopy (SEM). Top-view and cross-section experiments were carried out with an FEI XL40 Sirion FEG microscope operating at an acceleration voltage of 5 kV. The secondary electron image was collected in ultrahigh-resolution mode at a working distance of 5 mm.

Transmission Electron Microscopy (TEM). Block copolymer films on silicon wafers covered by a 100 nm thick layer of oxide were immersed in a 10 wt % HF solution and transferred to a water bath, floated off of the substrate, and placed on a Cu grid. Measurements were conducted with a FEI Tecnai G20 operating at 200 kV. Films were imaged either normal to or at various angles to the film plane to determine the three-dimensional lattice symmetry of the spherical domains.

X-ray Reflectivity. The total thickness of spin-coated films was measured by X-ray reflectivity using a Philips X'Pert MRD operating at a wavelength of 0.154 nm (Cu Kα). The reflectivity for each sample was fit using the Parratt procedure through the

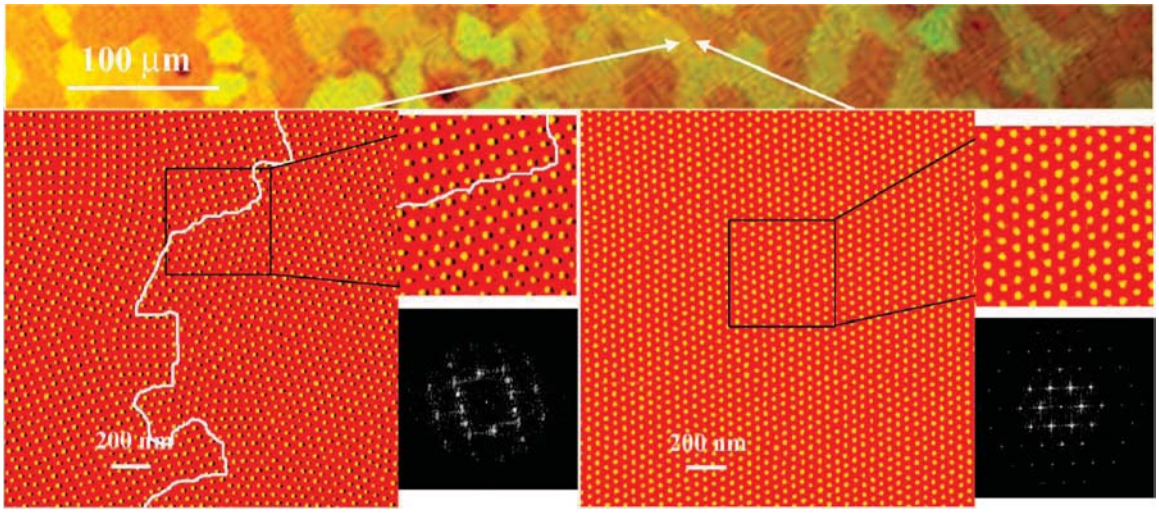

Figure 3. Surface structure of a PEO-*b*-PMMA-*b*-PS thin film with an overall thickness 117 nm after annealing for 16 h under saturated benzene vapor in high humidity. (upper) Optical micrograph of solvent-annealed film: arrow spans two regions: left region (lighter region) with square packing; right region (darker region) with hexagonal packing. (lower left) SFM phase image of coexisting hexagonal and square packing on the surface separated by a boundary between the two drawn for clarity as a white curve (inset: magnified area and corresponding Fourier transform). (lower right) SFM phase image of hexagonal packing on the surface (inset: magnified area and corresponding Fourier transform).

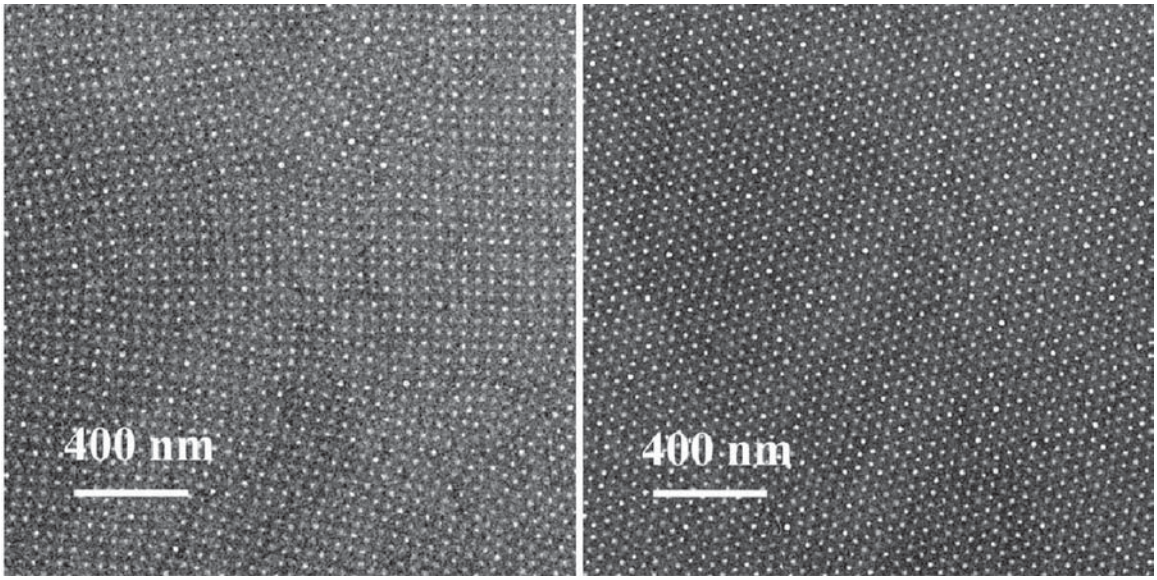

Figure 4. Plan-view bright field TEM images of PEO-*b*-PMMA-*b*-PS thin films with an as-spun thickness of 117 nm after annealing for 16 h under saturated benzene vapor in high humidity: (left) a region of square packing; (right) a region of hexagonal packing.

X'Pert Reflectivity simulation software to obtain the total film thickness.

Grazing Incidence Small-Angle X-ray Scattering (GISAXS). GISAXS experiments were conducted at the XOR Beamline 8-ID-E at the Advanced Photon Source (APS) of Argonne National Laboratory, at an X-ray energy of 7.35 keV ($\lambda = 0.1675$ nm). The sample is irradiated at a fixed incident angle on the order of a tenth of a degree, and the off-specular scattering is recorded with a 2D MAR-CCD detector with a resolution of 79 μm per pixel at a distance of 1900 mm from the sample. Exposure times under these conditions ranged from 1 to 30 s. Several measurements from each incident angle were summed to provide a signal well above the background. The strong specular reflection from the samples is blocked by a lead beam stop. Each data set is stored as a 2048 $\times$ 2048 16-bit TIFF image.

Results

The synthesis of well-defined ABC triblock copolymers PEO-*b*-PMMA-*b*-PS was reported earlier.[40] The copolymer chosen for this study has a 10% volume fraction of PMMA and 8% of PEO. Such low fractions of PMMA and PEO ensure the formation of spherical core/shell PEO/PMMA domains embedded in a PS matrix after solvent annealing. The ABC copolymer solution in benzene was spin-coated onto silicon substrates, and the thicknesses of the as-cast films investigated here were 43, 71, and 117 nm, corresponding to solution concentration 1.0, 1.5, and 2.5 wt %, respectively. These thicknesses were determined by X-ray reflectivity. The as-cast films were subjected to solvent annealing under saturated benzene vapor overnight followed by rapid solvent evaporation in a humid atmosphere with relative humidity controlled to ~80−90% at room temperature. After the solvent annealing process, the surface morphology of the films was visualized with the aid of high-resolution scanning force microscopy.

Figure 1 shows a 4 μm square SFM phase image from the 117 nm thick solvent-annealed films. The films exhibited mechanically lossy round features within the PS matrix with high orientational ordering. Grain sizes were in the range of

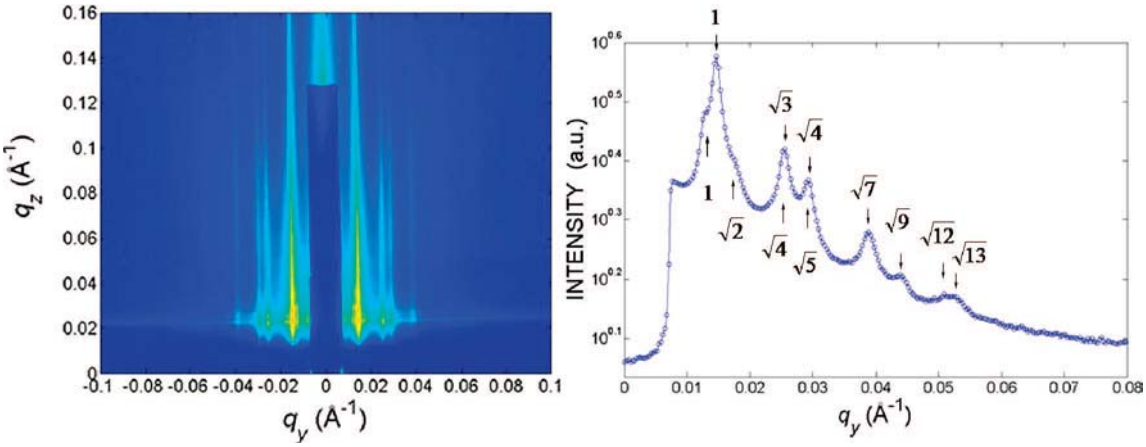

Figure 5. GISAXS pattern and scattering profile of a PEO-*b*-PMMA-*b*-PS thin film with an as-spun thickness of 117 nm, after annealing for 16 h under saturated benzene vapor and high humidity

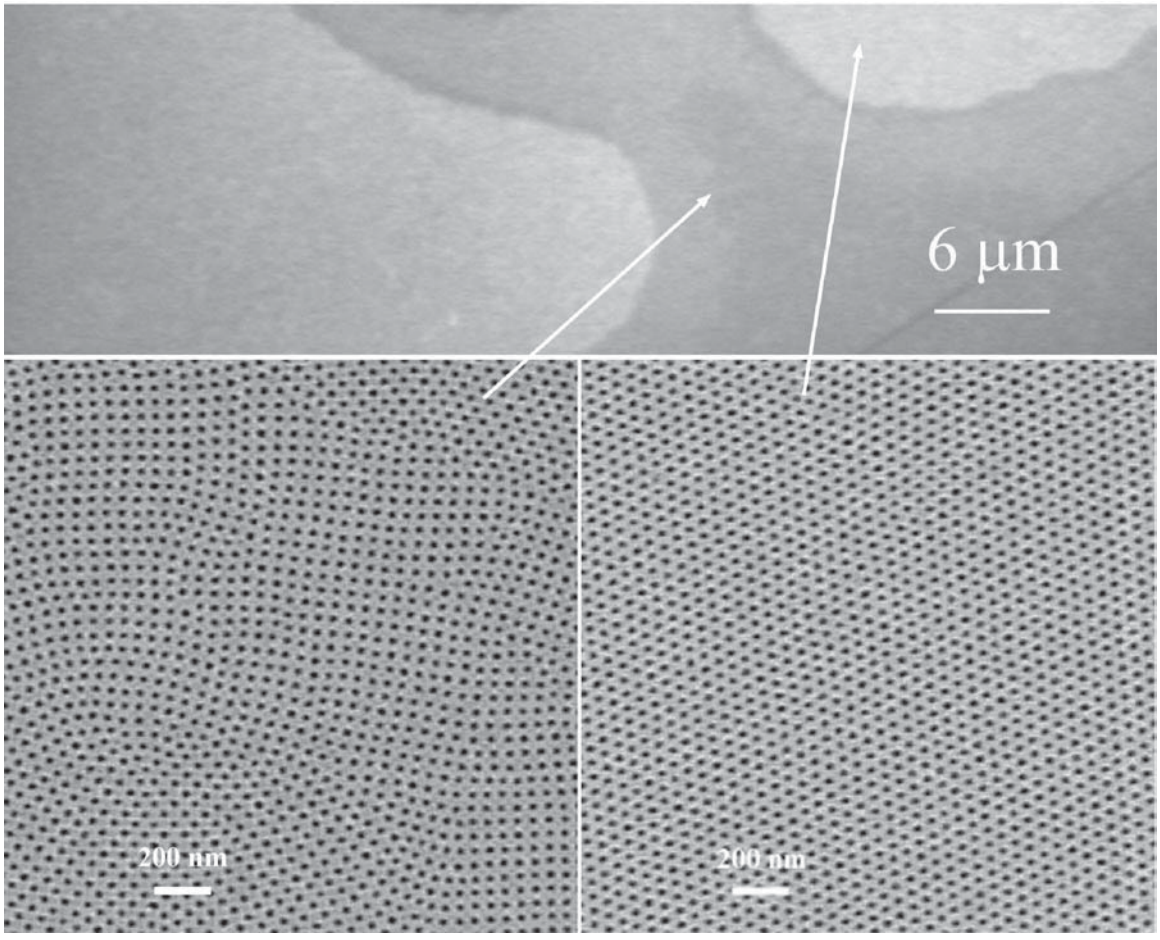

Figure 6. SEM images of a PEO-*b*-PMMA-*b*-PS thin film with an as-spun thickness of 117 nm after solvent annealing, UV degradation, and acid washing: (upper) large-scale top-view of films; (lower left) square packing; (lower right) hexagonal packing.

1−2 μm. Remarkably, the ordered domains exhibited square packing instead of the typical hexagonal ordering observed in most spherical or cylindrical block copolymer films. Magnified regions with very few defects on the surface of the thin films confirmed the formation of a single crystal of square domain arrays as indicated from the associated Fourier transform. Such unusual square packing was observed with repeated solvent annealing experiments under controlled high humidity. Imaging by both open-loop and closed-loop controlled scanners (Nanoscopic multimode vs MFP-3D) under different tapping conditions (light and hard tapping) excluded the possibility of the square packing being caused by tip artifacts or scanner piezo drift. We believe that this is the first time that square packing of domains has been observed on the surface of a single component ABC triblock copolymer. AB diblock copolymers or ABC triblock copolymers with cylinder domains, with cylinders normal to the film plane normally have a hexagonal arrangement on the surface, although square arrays of perpendicular cylinders in very thin films on square patterned substrates have been recently reported.[59] Initially, it was suspected that the PEO-*b*-PMMA-*b*-PS system in this study also adopted a "cylindrical structure" perpendicular to the surface. Further experimental evidence, as outlined in detail in the following sections, revealed that the surface domains were half-spheres,

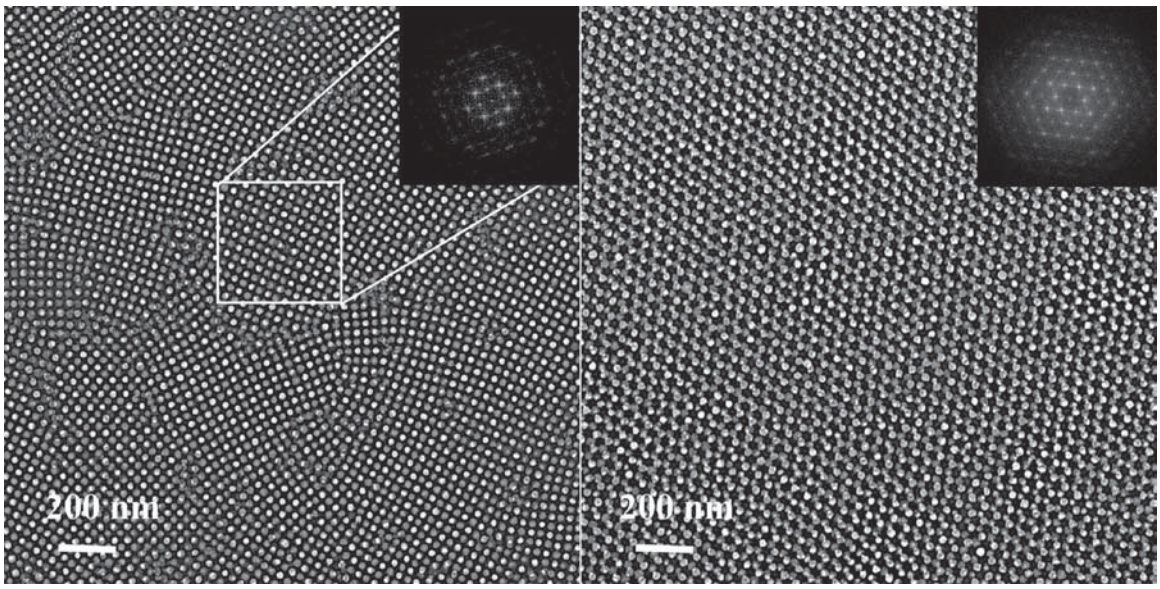

Figure 7. Bright field TEM plan-view images of a PEO-*b*-PMMA-*b*-PS thin film with a thickness as-spun of 117 nm after solvent annealing, UV degradation, and acid washing: (left) a region of square packing and (right) a region of hexagonal packing; (inset left) Fourier transform of magnified area; (inset right) Fourier transform of the whole image.

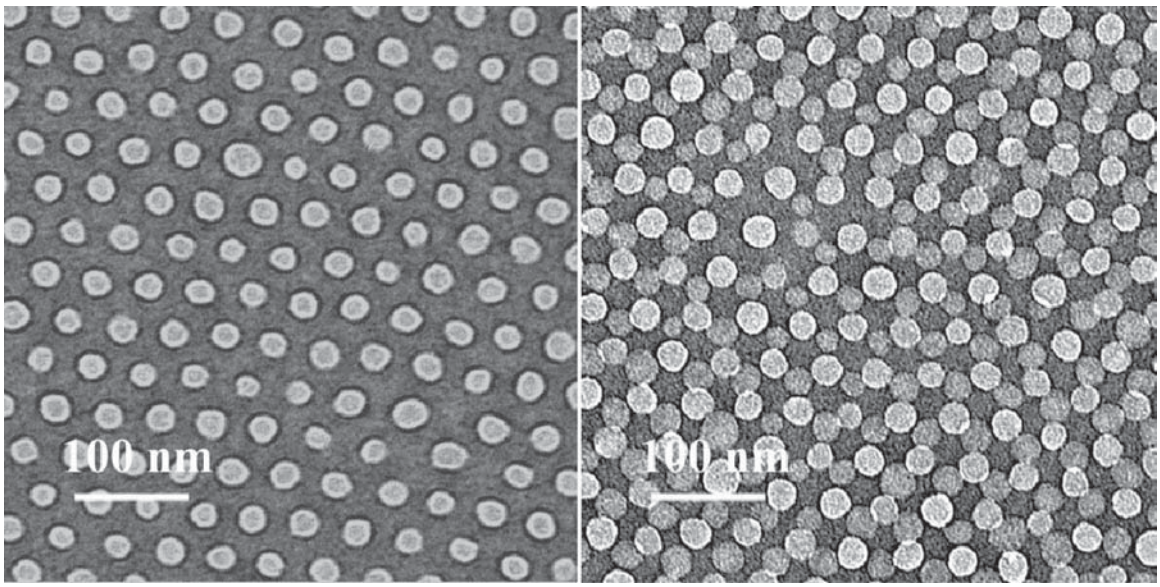

Figure 8. Bright field TEM plan-view images of PEO-*b*-PMMA-*b*-PS thin films after solvent annealing, UV degradation, and acid washing: (left) film thickness 43 nm; (right) film thickness 71 nm.

not cylinders, and that films with multiple layers consisted of $1^1/_2$ and $2^1/_2$ layers of spheres. SFM topography (Figure 2) under light tapping showed square arrays of circular depressions (1−3 nm deep) and 20 nm in diameter within a more rigid matrix. While these depressions could indicate the intersections of PEO-rich cylinder domains with the surface, the TEM results reported below show clearly that the domains are not cylinders.

In order to explore whether the square array occupied the entire film surface, we investigated the solvent-annealed films by optical microscopy. As shown in Figure 3, films after solvent annealing were rougher than the as-cast ones and displayed some regions that were thicker than others. Large-scale SFM topographic imaging along the boundary between two such regions revealed that the lighter regions in the optical image are slightly thinner (about 10−20 nm) than the darker regions. Considering the overall thickness of 117 nm determined by X-ray reflectivity, the thickness of the lighter and darker regions was estimated about 105 ± 5 and 125 ± 5 nm, respectively. Imaging in the lighter and darker regions revealed the formation of completely different packings: the thinner, lighter regions were dominated by square packing, while the thicker darker regions were mostly occupied by hexagonal packing. High-resolution SFM images (4096 pixel × 4096 pixel by MFP-3D) of the lighter regions (not shown) clearly showed the square arrays persisting at least 20 μm. Further imaging near the boundary between these two regions observed a clear structural transition between square and hexagonal packing as indicated by both phase images and associated Fourier transforms (Figure 3). It is worth noting that the grains of the hexagonal structure are larger than those of the square array.

The solvent-annealed films were subsequently characterized by TEM (Figure 4). Even without staining, distinct contrast between bright round features and a dark matrix were observed. No regions of intermediate contrast were observed even after staining the matrix PS with RuO_4. Our earlier work showed that under a humid atmosphere PMMA with molecular weight

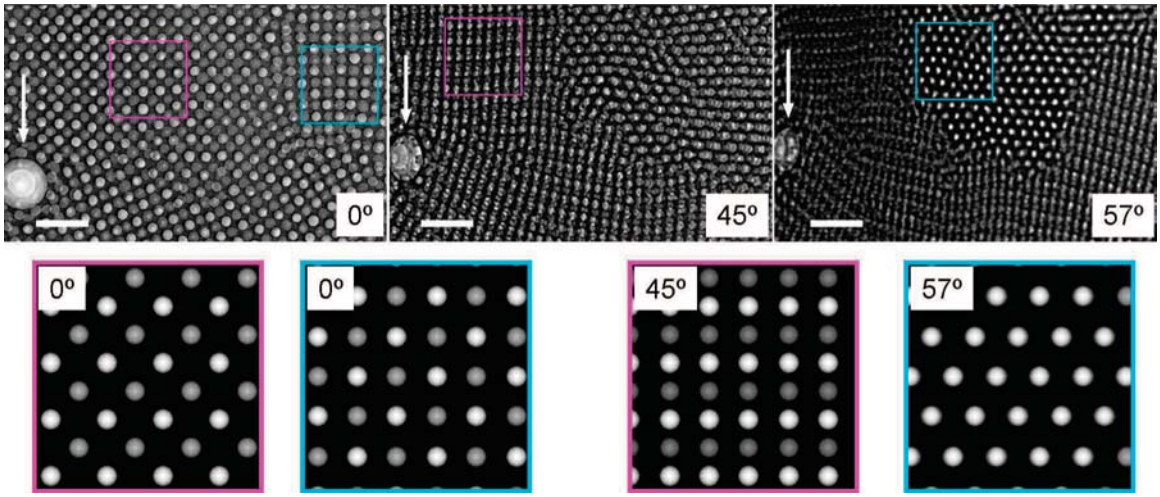

Figure 9. Bright field TEM tilting experiments (tilts of 0°, 45°, and 57°) and comparison with calculated projections for a BCC lattice of spheres. The images are from a PEO-*b*-PMMA-*b*-PS thin film with an as-spun thickness of 117 nm after solvent annealing, UV degradation, and acid washing (scale bar: 150 nm). The color frames represent different regions before and after tilting.

above 6000 g/mol should microphase separate from PEO segments with molecular weight 5000 g/mol. Given the PMMA molecular weight (6500 g/mol) of the current system, PEO and PMMA domains are expected to microphase separate to form a core−shell structure, especially in high-humidity conditions as water is a good solvent for PEO and a poor solvent for PMMA. We were not able to distinguish the PEO core and PMMA shell by TEM due to the low atomic number *Z* contrast between these two segments. Nevertheless, these microdomains showed highly ordered structures. TEM plan-view images also revealed two different packings: square and hexagonal. The center-to-center spacing of square and hexagonal arrays corresponds to 51 and 43 nm, respectively, which are in very good agreement with the SFM measurements. The TEM images also showed that the regions of hexagonal packing had a larger grain size than those of square packing.

SFM and TEM techniques are able to characterize the local structure of block copolymer thin films on a scale of up to tens of micrometers. In order to obtain a macroscopic understanding of the structures of these thin films, we utilized grazing incidence small-angle X-ray scattering (GISAXS). Solvent-annealed films, 117 nm thick, were exposed to monochromatic synchrotron X-radiation (energy 7.35 eV) at an incidence angle 0.185°, which is above the critical angle for total reflection (∼0.16°) of the polymer film but below the critical angle (∼0.22°) of the silicon substrate. As can be seen from the 2-D GISAXS patterns in Figure 5, the block copolymer films produced multiple streaklike scattering rods (offset in q_z and along the q_z direction normal to the plane), which seem to consist of two different scattering frameworks. Along the in-plane q_z direction seven strong relative scattering peaks observed are q^*_{hex}, $\sqrt{3}q^*_{hex}$, $\sqrt{4}q^*_{hex}$, $\sqrt{7}q^*_{hex}$,$\sqrt{9}q^*_{hex}$, $\sqrt{12}q^*_{hex}$, and $\sqrt{13}q^*_{hex}$, corresponding to an in-plane hexagonal packing. The two shoulders next to the strongest scattering peaks have scattering vectors of q^*_{sq} and $\sqrt{2}q^*_{sq}$. If we consider $\sqrt{3}q^*_{hex}$ and $\sqrt{4}q^*_{hex}$ peaks to overlap $\sqrt{4}q^*_{sq}$ and $\sqrt{5}q^*_{sq}$ peaks, respectively, the four additional scattering vectors have ratios with q^*_{sq} of 1, $\sqrt{2}$, $\sqrt{4}$, and $\sqrt{5}$, which are consistent with an in-plane square packing. The periodic spacing corresponding to the strongest maximum, and the left shoulder of Bragg rods is about 43 and 50 nm (q_y = 0.147 and 0.126 nm^{-1}), which are very close to those obtained from SFM and TEM measurements.

The solvent-annealed films were subjected to UV irradiation in order to partially cross-link the PS matrix and simultaneously degrade the PMMA domains, which were subsequently washed by acetic acid, yielding nanoporous films. Since the core PEO segments were connected to the PS with PMMA, they were potentially removed by acid washing simultaneously with the degraded PMMA residuals. SEM and TEM were used to investigate the plan-view structures of resulting nanoporous films. As shown in Figure 6, plan-view, large-scale SEM images of gold-coated UV-degraded films unambiguously revealed the formation of two different regions similar to those observed by SFM. The lighter regions were composed of hexagonally packed spheres, while darker regions consisted of square-packed porous arrays. The darker round features corresponded to electron-deficient nanopores, which were surrounded by cross-linked PS domains (lighter matrix). A similar structural transition (from square to hexagonal) at the boundary of these two regions was also observed (not shown).

TEM characterization of these nanoporous films revealed similarities and differences compared to as-solvent-annealed films without UV irradiation. First, these films had regions of two different packing structures, square and hexagonal, similar to those seen in the SFM and SEM results. Further observation of the films, however, indicated that there were three projected levels of contrast in TEM images of the domains of both square and hexagonal regions: dark, gray, and white (Figure 7). The dark, continuous regions are apparently cross-linked PS matrix. While the square-packed regions of as-solvent-annealed (not UV-degraded) films observed by SFM and TEM showed a simple square packing of circular domains, the TEM images of the square-packed regions in the nanoporous films reveal that each gray (white) domain is surrounded by four white (gray) domains. In the case of hexagonal packing, the gray and white regions consist of two alternate, almost perfect hexagonal arrangements, in which each gray (white) domain is surrounded by three white (gray) domains. However, the following TEM tilting and SEM cross-section experiments indicated that this packing is actually a result of stacking of multilayers of spheres in conjunction with half-spheres at the film surface.

The above experiments were focused on the films with a thickness of 117 nm. Films with thickness 43 and 71 nm were also characterized by similar techniques. On the surface, both films after solvent annealing produced hexagonal structural packing as observed by SFM, SEM, and GISAXS. No square packing was observed. After UV degradation and acid washing, these structures preserved their original hexagonal packing. For films with thickness 43 nm, only white round features and dark matrix were observed in the TEM images (Figure 8), which

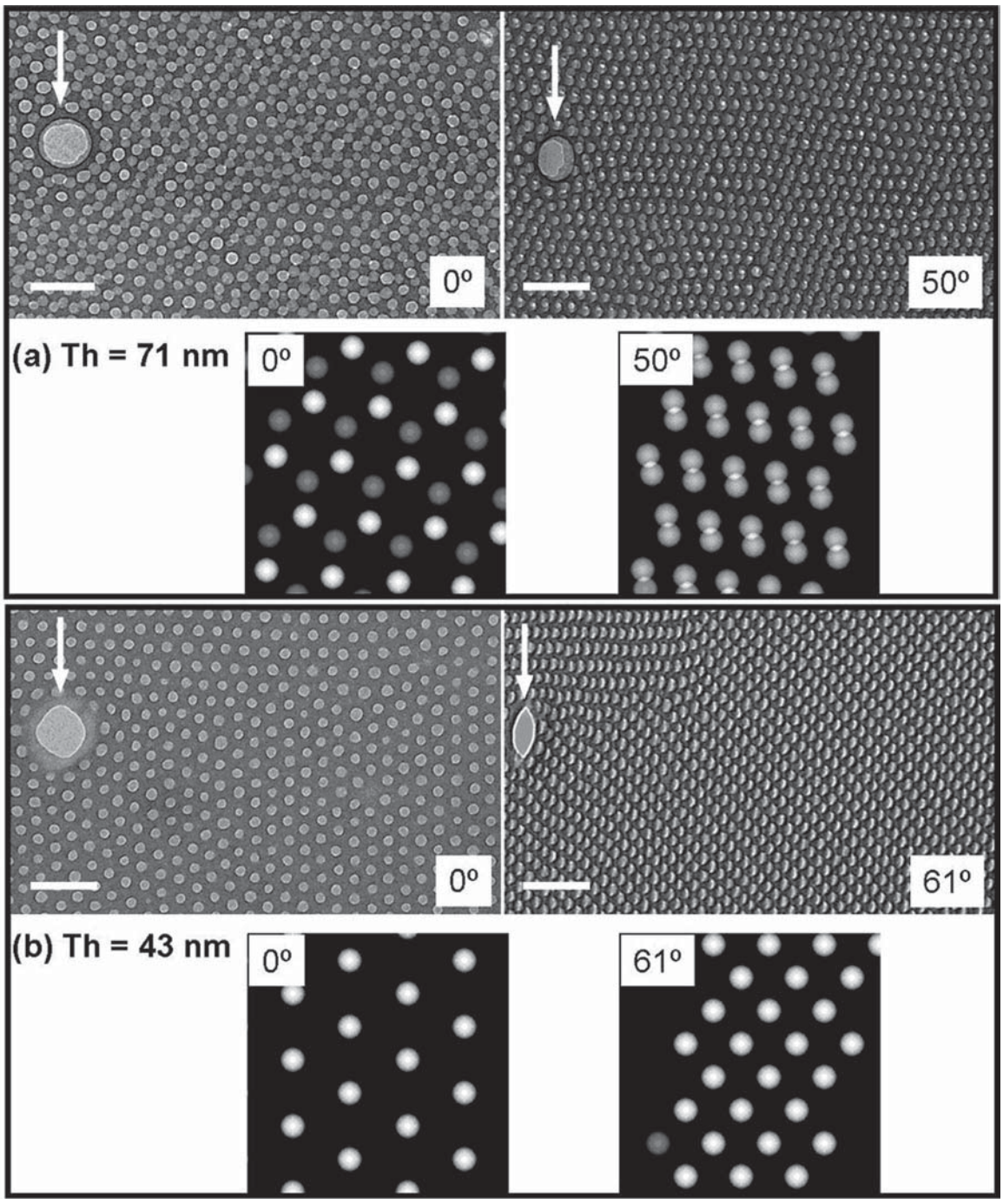

Figure 10. Bright field TEM tilting experiments and comparison with calculated projections for hexagonal lattice of PEO-*b*-PMMA-*b*-PS thin films with thickness (a) 71 nm and (b) 43 nm after solvent annealing, UV degradation, and acid washing (scale bar: 150 nm).

are similar to the TEM images of as-solvent-annealed films without UV irradiation, although the contrast between the two regions was stronger due to higher *Z* contrast after UV degradation. Films 71 nm thick after UV irradiation had three different regions, similar to those observed from 117 nm thick films subject to the same treatment.

In order to understand the complex structures observed by SFM, TEM, and SEM plan-view studies and to further characterize the 3-dimensional internal structures of the films, we carried out TEM tilting and SEM cross-section experiments on nanoporous films. Figure 9 shows the films with thickness 117 nm tilted at 0° (plan view), 45°, and 57°. A region with an artifact (shown by the arrow) was chosen intentionally in order to mark the region so that it could be followed and kept in view while tilting. For films tilted at any angle (images from other angles are not shown), no elongated features were observed, indicating that the films consisted of spheres rather than cylinders. Two different regions were carefully tracked as marked with purple and blue frames in Figure 9. Simulated TEM images for different assumed structures were compared with the experimental images. The calculated projections assumed 2 layers of full spheres and 1 layer of half-spheres at the surface. The 45° view is a rotation about a ⟨001⟩ axis and corresponds to a ⟨110⟩ projection, while the 57° view is a rotation about a $\langle 0\bar{1}1\rangle$ axis and corresponds to a ⟨111⟩ projection of the BCC layer. The simulated structures are in good agreement with experimental data, indicating the buried spheres (and surface half-sphere) are organized on a BCC lattice with its (100) plane parallel to the film surface.

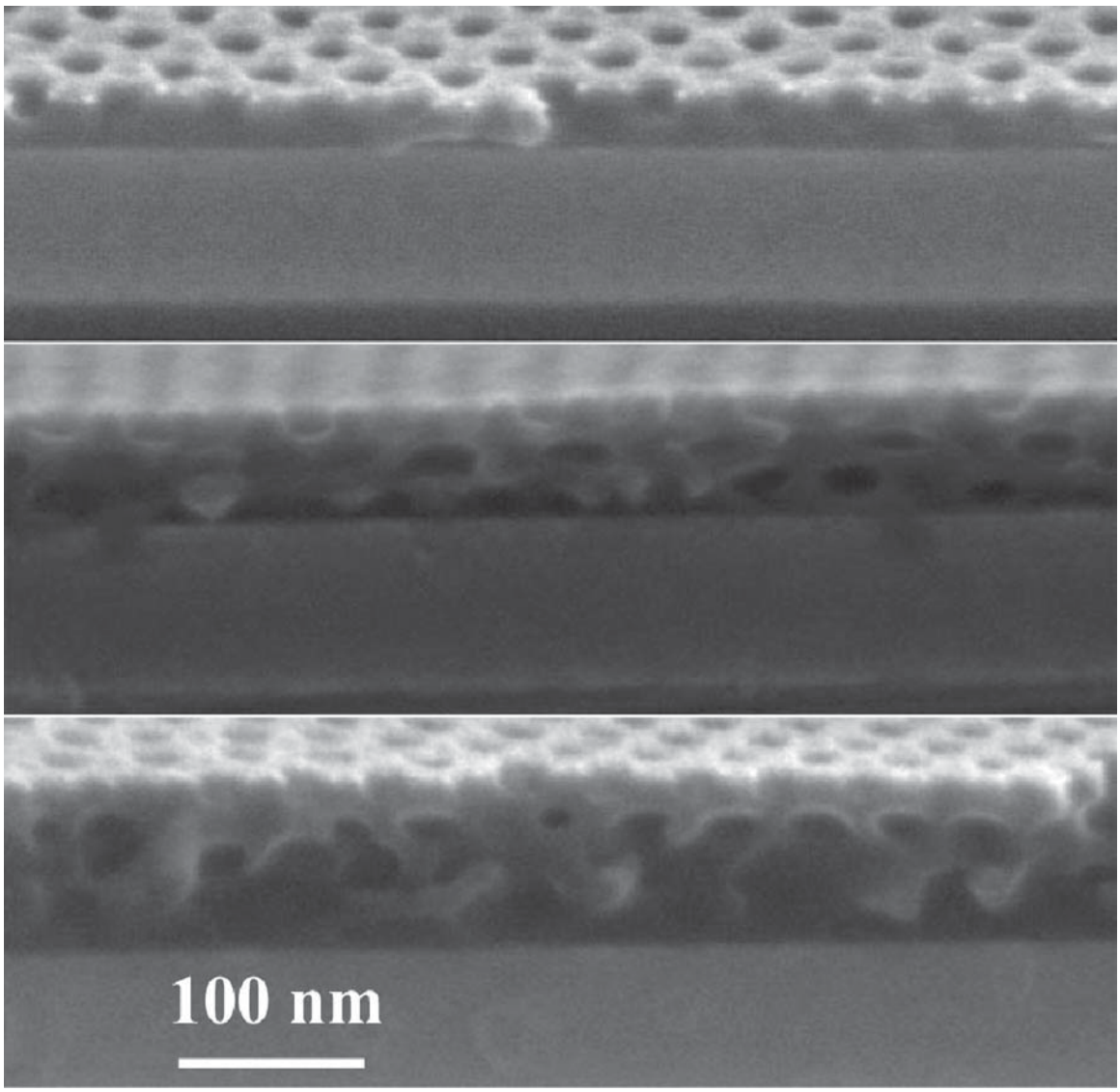

Figure 11. Cross-section SEM images of PEO-*b*-PMMA-*b*-PS thin films after solvent annealing, UV degradation and acid washing: (upper) film thickness 43 nm; (middle) film thickness 71 nm; (lower) film thickness 117 nm.

Figure 10 compares the simulated structures with experimental observations of films with thicknesses of 71 and 43 nm. The films 43 nm thick were clearly composed of one layer of hexagonally arranged half-spheres as no second layer was observed after tilting. Note that the large hole artifact on the left of the image is brighter than the half-spheres since these spheres do not penetrate through the film. Films 71 nm thick, however, contained one layer of full spheres and one layer of half-spheres, again with a hexagonal lattice, which exhibited an AB stacking.

As shown in Figure 11, cross-section SEM images confirmed that no porous channels from the surface to the substrate were observed, indicating these ordered pores are not cylinders. These images further demonstrated that concave half-spherical pores were formed on the surface of each film. The pore on the surface is empty, indicating the efficient UV degradation and acetic acid washing. Films only 43 nm thick exhibited one layer of half-sphere pores on the surface, consistent with a monolayer of half-spheres observed by TEM tilting experiments. Films 71 nm thick consisted of a half-sphere layer on the surface and a full layer embedded underneath, which is in good agreement with the tilting experiments. Films 117 nm thick had a half-sphere layer on the surface and two layers embedded in the matrix underneath.

Discussion

The TEM tilt series and the SEM cross sections reveal that the PEO-*b*-PMMA-*b*-PS thin films consist of a surface layer of PEO spheres plus layers of whole spheres whose number and in-plane structure depend on film thickness. This raises interesting questions such as why half-spheres are present on the surface of all films. In addition, why for a unique thickness is a BCC structure with the (100) parallel to the surface observed when for thicknesses both below and above that a hexagonal structure is seen?

In order to answer these questions, one must address the mechanisms of the formation of block copolymer thin film morphology as a result of solvent annealing under high humidity. The fact that the hydrophilic PEO block domains,[40] or blocks that are expected to prefer to include PEO additives,[42] are located at the surface of films formed by rapid evaporation of the solvent only under high-humidity conditions, even though the surface energy of PEO is higher than the PS matrix, suggests the critical role of water. While the exact mechanism is not yet completely clear, we reason that there are two possible mechanisms. In the first mechanism water absorption would lead to an increased effective Flory−Huggins parameter χ between water and solvent containing PEO domains and other two

Scheme 2. Illustration of Proposed Structures of (a) Monolayer, (b) Bilayer, and (c, d) Triple Layer of PEO-*b*-PMMA-*b*-PS Thin Film: (Left) Top View; (Middle) Cross-Sectional View of the Film Packing; (Right) Chain Configurations

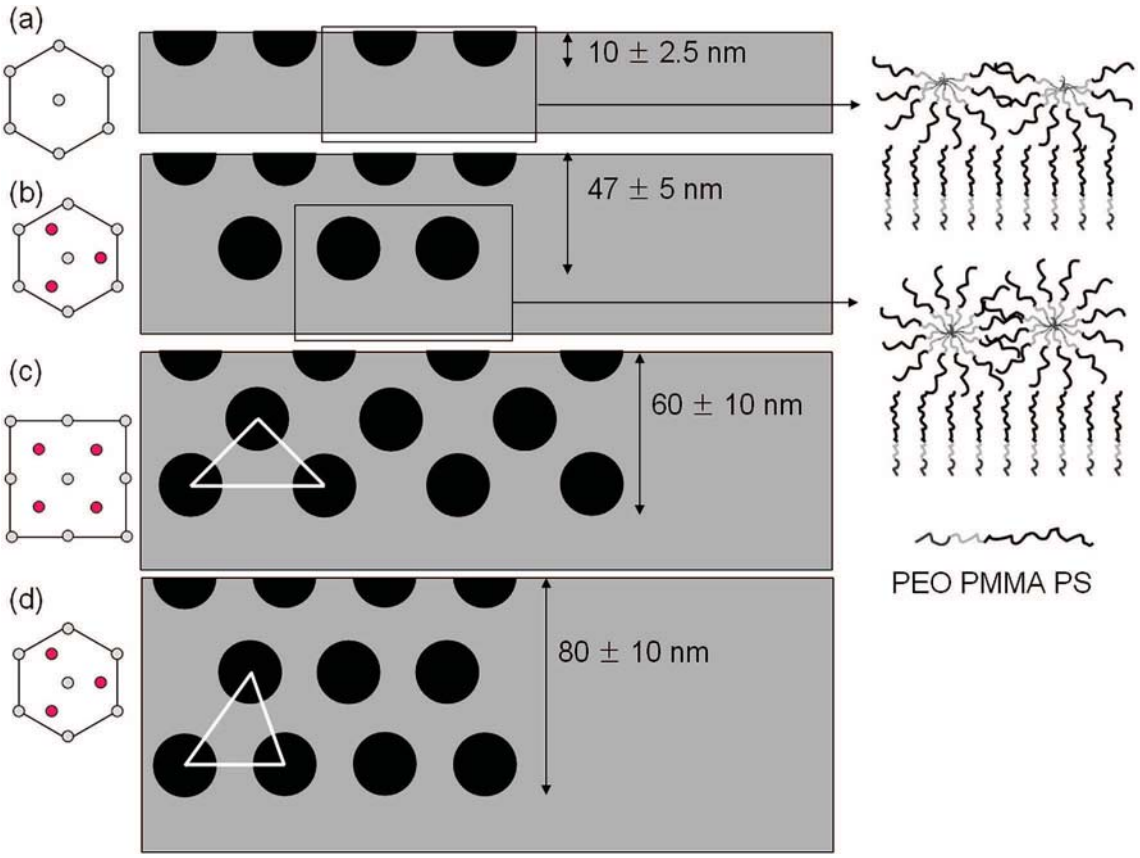

solvent swollen domains. When the films are exposed to the humid atmosphere, the water primarily swells the hydrophilic PEO domains, perhaps expelling some of the benzene solvent from these. Such swelling would drive microphase separation at the surface where the solvent concentration is the lowest as the solvent evaporates. The gradient of solvent concentration perpendicular to the surface would be a driving force to cause the microphase separation to propagate directionally from the surface down into the whole film.[37–39] In this scenario the lateral order of domains at the surface develops while the film is still swollen, even perhaps before the evaporation of solvent begins.[60,61] The increasing interaction between PEO and PMMA under high humidity was confirmed by the microphase separation observed in an earlier report.[40,41] In the melt, PEO and PMMA segments are miscible with χ close to 0. The other possible mechanism could be analogous to the widely observed breath figure (BF) formation on drop-cast polymer films.[62–72] In earlier publications,[41,42] we proposed the possibility that water condensation onto the PEO-based block copolymers leads to PEO domain ordering. After solvent annealing, the solvent evaporation causes the cooling of the film surface. As cooling proceeds, PEO concentrations near the swollen film surface could lead to heterogeneous nucleation of very small water droplets. These water droplets attract other hydrophilic PEO chains, leading to water swollen PEO block domains at the surface. The tiny water droplets are attracted to each other by any deformation of the swollen film surface they caused, by the flow of solvent vapor between them, and even by van der Waals forces. However, if the droplets with their water swollen PEO domains approach each other too closely, they are repelled by the solvent swollen PS-*b*-PMMA corona brush attached to the PEO domain. This combination of attractive forces at long range and repulsive forces at short range could give rise to the ordering of the PEO surface. The first layer of water swollen PEO domains can then act as a template to control the packing of buried layers, yielding a multilayer ordered structure. Once water evaporates from the PEO domains (the water is much less volatile than the solvent and thus leaves last), a layer of half-spheres of PEO is created on the surface but with an indentation in its center due to the removal of the water. It is possible that one or the other or even both of these mechanisms operates in this case; further experiments will be necessary to distinguish between them. However, it is clear that in some cases, i.e., block copolymers of isoprene and polylactic acid, that solvent annealing under conditions that produce just the correct swelling by the solvent that water is unnecessary, and thus the first mechanism presumably operates.[60,61]

The packing of spheres on the surface will be influenced by the film thickness as it increases from monolayer to multilayer dimensions. When the thickness is not commensurate with the stacking of the layered structure in thermally equilibrated films, the formation of islands and holes is usually observed. Under the solvent swollen conditions obtaining in solvent annealing, the large surface tension makes it very difficult to form full height islands or holes in the hexagonal structured film. As shown in Figure 3, the films with the as-spun thickness of 117 nm exhibited characteristic thickness variations in order to accommodate the formation of different layered structures. It has been established that the equilibrium lattice structure of spheres in thin films is the one that minimizes the unfavorable conformations arising from the deformation of the longest chains to uniformly fill the matrix space.[27] For thermally equilibrated diblock copolymer films 4 layers or less thick, spheres pack on a HCP lattice.[30] Our results for the solvent annealed PEO-*b*-PMMA-*b*-PS films where solvent is evaporated under high-humidity conditions are different. For thin films containing a single layer of half-spheres (43 nm thick) or a layer of half-spheres and a layer of full spheres (71 nm thick), the lattice is

hexagonal. Assuming the diameter of the spheres and the thickness of a wetting layer on the substrate are 20 ± 5 and 30 ± 5 nm, respectively, the thickness of a layer of half-spheres would be 10 ± 2.5 nm plus brush of PS-*b*-PMMA attached to the spheres, and the thickness of a layer of half-spheres and a layer of full spheres would be 47 ± 5 nm, as shown in Scheme 2a,b. However, when the films reach three layers, the fact that the initial thickness is not exactly commensurate with the thickness of any of the structures results in coexistence of two different structures so as not to require nucleation of full thickness holes of the hexagonal structure. A BCC structure is observed in some regions of the films that were 117 nm thick as-spun. Hexagonal packing (Scheme 2d) is no longer the only arrangement on the surface, particularly in thinner regions of the films. In such regions, the film adopts a square packing of PEO spheres on the surface corresponding to the (100) plane of an underlying BCC structure as shown in Scheme 2c.

Conclusions

Thin films of spherical core/shell ABC triblock copolymers were treated by solvent annealing under high humidity and subsequently irradiated by UV light to degrade PMMA segments. These films were investigated with the aid of scanning force microscopy, scanning electron microscopy, transmission electron microscopy, and grazing incidence small-angle X-ray scattering. The structure packing on the surface is strongly influenced by the film thickness. Monolayer (layer of half-spheres) and bilayer ($1^1/_2$ layers of spheres) films were shown to have a close-packed hexagonal structure. Films with 3 layers ($2^1/_2$ layers of spheres) exhibited coexistence of a close-packed hexagonal structure (in thick regions) and a square packing structure corresponding to the (100) plane of an underlying body-centered cubic (BCC) lattice (in thinner regions). A half-sphere layer was formed on the surface of all the films. Both half-sphere and ordered structures on the surface are believed to be a result of interaction between highly hydrophilic PEO segments and water under solvent evaporation and perhaps simultaneous water condensation.

Acknowledgment. This work was supported by the Nanoelectronics Research Initiative under contract RID#1549 (SRC/NRI) and the National Science Foundation under the MRSEC program (UCSB MRL, DMR-0520415). Additional support from the NSF Polymer Program Award DMR-0704539 is also acknowledged. Use of the APS was supported by the US DOE Office of Basic Energy Sciences, under contract DE-AC02-06CH11357.

References and Notes

(1) Fredrickson, G. H.; Bates, F. S. *Annu. Rev. Mater. Sci.* **1996**, *26*, 501–550.
(2) Hadjichristidis, N.; Pispas, S.; Floudas, G. *Block Copolymers: Synthetic Strategies, Physical Properties, and Applications*; John Wiley & Sons: Hoboken, NJ, 2003.
(3) Ross, C. *Annu. Rev. Mater. Res.* **2001**, *31*, 203–235.
(4) Park, M.; Harrison, C.; Chaikin, P. M.; Register, R. A.; Adamson, D. H. *Science* **1997**, *276*, 1401–1404.
(5) Hawker, C. J.; Russell, T. P. *MRS Bull.* **2005**, *30*, 952–966.
(6) Bates, F. S.; Fredrickson, G. H. *Phys. Today* **1999**, *52*, 32–38.
(7) Bates, F. S.; Fredrickson, G. H. *Annu. Rev. Phys. Chem.* **1990**, *41*, 525–557.
(8) Segalman, R. A. *Mater. Sci. Eng. R* **2005**, *R48*, 191–226.
(9) Cheng, J. Y.; Ross, C. A.; Smith, H. I.; Thomas, E. L. *Adv. Mater.* **2006**, *18*, 2505–2521.
(10) Morkved, T. L.; Lu, M.; Urbas, A. M.; Ehrichs, E. E.; Jaeger, H. M.; Mansky, P.; Russell, T. P. *Science* **1996**, *273*, 931–933.
(11) Segalman, R. A.; Yokoyama, H.; Kramer, E. J. *Adv. Mater.* **2001**, *13*, 1152–1155.
(12) Cheng, J. Y.; Ross, C. A.; Thomas, E. L.; Smith, H. I.; Vancso, G. J. *Appl. Phys. Lett.* **2002**, *81*, 3657–3659.
(13) Albalak, R. J.; Thomas, E. L. *J. Polym. Sci., Polym. Phys.* **1994**, *32*, 341–350.
(14) Angelescu, D. E.; Waller, J. H.; Register, R. A.; Chaikin, P. M. *Adv. Mater.* **2004**, *16*, 1736–1740.
(15) Ryu, D. Y.; Shin, K.; Drockenmuller, E.; Hawker, C. J.; Russell, T. P. *Science* **2005**, *308*, 236–239.
(16) Mansky, P.; Liu, Y.; Huang, E.; Russell, T. P.; Hawker, C. J. *Science* **1997**, *275*, 1458–1460.
(17) Kim, S. O.; Solak, H. H.; Stoykovich, M. P.; Ferrier, N. J.; de Pablo, J. J.; Nealey, P. F. *Nature (London)* **2003**, *424*, 411–414.
(18) Kimura, M.; Misner, M. J.; Xu, T.; Kim, S. H.; Russell, T. P. *Langmuir* **2003**, *19*, 9910–9913.
(19) Tang, C.; Tracz, A.; Kruk, M.; Zhang, R.; Smilgies, D.-M.; Matyjaszewski, K.; Kowalewski, T. *J. Am. Chem. Soc.* **2005**, *127*, 6918–6919.
(20) De Rosa, C.; Park, C.; Thomas, E. L.; Lotz, B. *Nature (London)* **2000**, *405*, 433–437.
(21) Kinning, D. J.; Thomas, E. L. *Macromolecules* **1984**, *17*, 1712–1718.
(22) Cheng, J. Y.; Ross, C. A.; Thomas, E. L.; Smith, H. I.; Vancso, G. J. *Adv. Mater.* **2003**, *15*, 1599–1602.
(23) Cheng, J. Y.; Zhang, H.; Smith, H. I.; Vancso, G. J.; Ross, C. A. *Adv. Mater.* **2006**, *18*, 597–601.
(24) Chuang, V. P.; Cheng, J. Y.; Savas, T. A.; Ross, C. A. *Nano Lett.* **2006**, *6*, 2332–2337.
(25) Bates, F. S.; Cohen, R. E.; Berney, C. V. *Macromolecules* **1982**, *15*, 589–592.
(26) Pedemonte, E.; Turturro, A.; Bianchi, V.; Devetta, P. *Polymer* **1973**, *14*, 145–150.
(27) Thomas, E. L.; Kinning, D. J.; Alward, D. B.; Henkee, C. S. *Macromolecules* **1987**, *20*, 2934–2939.
(28) Matsen, M. W. *J. Phys.: Condens. Matter* **2002**, *14*, R21–R47.
(29) Yokoyama, H.; Mates, T. E.; Kramer, E. J. *Macromolecules* **2000**, *33*, 1888–1898.
(30) Stein, G. E.; Kramer, E. J.; Li, X.; Wang, J. *Macromolecules* **2007**, *40*, 2453–2460.
(31) Stein, G. E.; Cochran, E. W.; Katsov, K.; Fredrickson, G. H.; Kramer, E. J.; Li, X.; Wang, J. *Phys. Rev. Lett.* **2007**, *98*, 158302.
(32) Kim, G.; Libera, M. *Macromolecules* **1998**, *31*, 2569–2577.
(33) Kim, G.; Libera, M. *Macromolecules* **1998**, *31*, 2670–2672.
(34) Hahm, J.; Sibener, S. J. *Langmuir* **2000**, *16*, 4766–4769.
(35) Fukunaga, K.; Elbs, H.; Magerle, R.; Krausch, G. *Macromolecules* **2000**, *33*, 947–953.
(36) Fukunaga, K.; Hashimoto, T.; Elbs, H.; Krausch, G. *Macromolecules* **2002**, *35*, 4406–4413.
(37) Kim, S. H.; Misner, M. J.; Xu, T.; Kimura, M.; Russell, T. P. *Adv. Mater.* **2004**, *16*, 226–231.
(38) Kim, S. H.; Misner, M. J.; Russell, T. P. *Adv. Mater.* **2004**, *16*, 2119–2123.
(39) Zhang, M.; Yang, L.; Yurt, S.; Misner, M. J.; Chen, J.-T.; Coughlin, E. B.; Venkataraman, D.; Russell, T. P. *Adv. Mater.* **2007**, *19*, 1571–1576.
(40) Bang, J.; Kim, S. H.; Drockenmuller, E.; Misner, M. J.; Russell, T. P.; Hawker, C. J. *J. Am. Chem. Soc.* **2006**, *128*, 7622–7629.
(41) Bang, J.; Kim, B. J.; Stein, G. E.; Russell, T. P.; Kramer, E. J.; Hawker, C. J. *Macromolecules* **2007**, *40*, 7019–7025.
(42) Park, S. C.; Kim, B. J.; Hawker, C. J.; Kramer, E. J.; Bang, J.; Ha, J. S. *Macromolecules* **2007**, *40*, 8119–8124.
(43) Segalman, R. A.; Yokoyama, H.; Kramer, E. J. *Adv. Mater.* **2001**, *13*, 1152–1155.
(44) Segalman, R. A.; Hexemer, A.; Kramer, E. J. *Phys. Rev. Lett.* **2003**, *91*, 196101.
(45) Segalman, R. A.; Hexemer, A.; Kramer, E. J. *Macromolecules* **2003**, *36*, 6831–6839.
(46) Segalman, R. A.; Schaefer, K. E.; Fredrickson, G. H.; Kramer, E. J.; Magonov, S. *Macromolecules* **2003**, *36*, 4498–4506.
(47) Segalman, R. A.; Hexemer, A.; Hayward, R. C.; Kramer, E. J. *Macromolecules* **2003**, *36*, 3272–3288.
(48) Stein, G. E.; Lee, W. B.; Fredrickson, G. H.; Kramer, E. J.; Li, X.; Wang, J. *Macromolecules* **2007**, *40*, 5791–5800.
(49) Stein, G. E.; Kramer, E. J.; Li, X.; Wang, J. *Phys. Rev. Lett.* **2007**, *98*, 086101.
(50) Mogi, Y.; Nomura, M.; Kotsuji, H.; Ohnishi, K.; Matsushita, Y.; Noda, I. *Macromolecules* **1994**, *27*, 6755–6760.
(51) Mogi, Y.; Kotsuji, H.; Kaneko, Y.; Mori, K.; Matsushita, Y.; Noda, I. *Macromolecules* **1992**, *25*, 5408–5411.
(52) Nakazawa, H.; Ohta, T. *Macromolecules* **1993**, *26*, 5503–5511.
(53) Chen, H.-Y.; Fredrickson, G. H. *J. Chem. Phys.* **2002**, *116*, 1137–1146.
(54) Xia, J.; Sun, M.; Qiu, F.; Zhang, H.; Yang, Y. *Macromolecules* **2005**, *38*, 9324–9332.
(55) Matsen, M. W. *J. Chem. Phys.* **1998**, *108*, 785–796.
(56) Bailey, T. S.; Pham, H. D.; Bates, F. S. *Macromolecules* **2001**, *34*, 6994–7008.
(57) Rzayev, J.; Hillmyer, M. A. *Macromolecules* **2005**, *38*, 3–5.
(58) Rzayev, J.; Hillmyer, M. A. *J. Am. Chem. Soc.* **2005**, *127*, 13373–13379.

(59) Park, S. M.; Craig, G. S. W.; La, Y. H.; Solak, H. H.; Nealey, P. F. *Macromolecules* **2007**, *40*, 5084–5094.
(60) Cavicchi, K. A.; Berthiaume, K. J.; Russell, T. P. *Polymer* **2005**, *46*, 11635–11639.
(61) Cavicchi, K. A.; Russell, T. P. *Macromolecules* **2007**, *40*, 1181–1186.
(62) Widawski, G.; Rawiso, M.; Francois, B. *Nature (London)* **1994**, *369*, 387–389.
(63) Srinivasarao, M.; Collings, D.; Philips, A.; Patel, S. *Science* **2001**, *292*, 79–83.
(64) Bunz, U. H. F. *Adv. Mater.* **2006**, *18*, 973–989.
(65) Steyer, A.; Guenoun, P.; Beysens, D.; Knobler, C. M. *Phys. Rev. B* **1990**, *42*, 1086–1089.
(66) Steyer, A.; Guenoun, P.; Beysens, D. *Phys. Rev. E* **1993**, *48*, 428–431.
(67) Pitois, O.; Francois, B. *Eur. Phys. J. B* **1999**, *8*, 225–231.
(68) Saunders, A. E.; Dickson, J. L.; Shah, P. S.; Lee, M. Y.; Lim, K. T.; Johnston, K. P.; Korgel, B. A. *Phys. Rev. E* **2006**, *73*, 031608.
(69) Limaye, A. V.; Narhe, R. D.; Dhote, A. M.; Ogale, S. B. *Phys. Rev. Lett.* **1996**, *76*, 3762–3765.
(70) Haupt, M.; Miller, S.; Sauer, R.; Thonke, K.; Mourran, A.; Moeller, M. *J. Appl. Phys.* **2004**, *96*, 3065–3069.
(71) Tian, Y.; Dai, C.; Ding, H.; Jiao, Q.; Wang, L.; Shi, Y.; Liu, B. *Polym. Int.* **2007**, *56*, 834–839.
(72) Chan, D. Y. C.; Henry, J. D.; White, L. R. *J. Colloid Interface Sci.* **1981**, *79*, 410–418.

MA800207N